

MIT Open Access Articles

*Optical bistability with a repulsive optical force
in coupled silicon photonic crystal membranes*

The MIT Faculty has made this article openly available. **Please share**
how this access benefits you. Your story matters.

Citation: Hui, Pui-Chuen, David Woolf, Eiji Iwase, Young-Ik Sohn, Daniel Ramos, Mughees Khan, Alejandro W. Rodriguez, Steven G. Johnson, Federico Capasso, and Marko Loncar. "Optical bistability with a repulsive optical force in coupled silicon photonic crystal membranes." Applied Physics Letters 103, no. 2 (2013): 021102.

As Published: <http://dx.doi.org/10.1063/1.4813121>

Publisher: American Institute of Physics (AIP)

Persistent URL: <http://hdl.handle.net/1721.1/81252>

Version: Author's final manuscript: final author's manuscript post peer review, without publisher's formatting or copy editing

Terms of use: Creative Commons Attribution-Noncommercial-Share Alike 3.0



Optical bistability with a repulsive optical force in coupled silicon photonic crystal membranes

Pui-Chuen Hui(),¹ David Woolf,¹ Eiji Iwase,² Young-Ik Sohn,¹ Daniel Ramos,¹ Mughees Khan,³ Alejandro W. Rodriguez,^{4, a)} Steven G. Johnson,⁴ Federico Capasso,¹ and Marko Loncar¹

¹⁾*School of Engineering and Applied Sciences, Harvard University, Cambridge, MA 02138 USA*

²⁾*Department of Applied Mechanics and Aerospace Engineering, Waseda University, Tokyo, Japan 169-8555.*

³⁾*Wyss Institute for Biologically Inspired Engineering, Harvard University, Boston, MA 02115.*

⁴⁾*Department of Mathematics, Massachusetts Institute of Technology, Cambridge, MA 02139 USA.*

(Dated: 27 May 2013)

We demonstrate actuation of a silicon photonic crystal membrane with a repulsive optical gradient force. The extent of the static actuation is extracted by examining the optical bistability as a combination of the optomechanical, thermo-optic and photo-thermo-mechanical effects using coupled-mode theory. Device behavior is dominated by a repulsive optical force which results in displacements of ≈ 1 nm/mW. By employing an extended guided resonance which effectively eliminates multi-photon thermal and electronic nonlinearities, our silicon-based device provides a simple, non-intrusive solution to extending the actuation range of MEMS devices.

PACS numbers: Pacs Here

Keywords: Keywords Here

^{a)}Also at Department of Mathematics, Massachusetts Institute of Technology, Cambridge, MA 02139 USA.

Rapid developments in the field of optomechanics have opened up avenues for fundamental research on quantum state manipulation with macroscopic structures¹ and show promise for novel optomechanical sensors² and technologies for both radio-frequency³ and telecom applications.⁴ While most attention has been devoted to compact structures featuring low (picogram) mass and ultrahigh-frequency (gigahertz) mechanical modes,^{5,6} the technological implications of static deformation due to optical forces have been less explored.⁷ In coupled photonic waveguide geometries,^{8,9} bonding and anti-bonding optical modes are supported and the corresponding attractive and repulsive optical forces exerted on a pliant structure (low mechanical frequency) could serve to broaden the range of motion of integrated microelectromechanical devices. This translates to improvement in the detection range of pressure and displacement sensors and the actuation range of electrostatic actuators. In particular, the pull-in limit of electrostatic actuators could be extended by increasing the plate separation with a repulsive optical force. Additionally, novel schemes for preventing stiction, which occurs when attractive forces like the Casimir force and electrostatic force become overwhelmingly large compared to the mechanical restoring force, have been proposed¹⁰ using a real-time monitoring of the structure's displacement and a counteracting feedback repulsive force (of the order of nano-Newtons and linear with excitation power). In this paper, we demonstrate nanometer-pulling of a thin silicon photonic crystal (PhC) membrane under low vacuum with a repulsive optical gradient force and an attractive photo-thermo-mechanical force. Furthermore, optical bistability induced by optical forces and thermo-optic effect is observed with large excitation powers while minimizing multi-photon nonlinearities.

Our devices – one of which is described in Fig. 1(a) and pictured in Fig. 1(c) – consist of a square silicon PhC slab suspended by four support arms ≈ 250 nm above a Silicon-on-Insulator (SOI) substrate. They are fabricated from a double-SOI platform, formed by oxide-oxide bonding of two thermally oxidized SOI wafers.

A sacrificial silicon dioxide layer between the two silicon layers is $s_0 = 265$ nm thick. Electron-beam lithography is performed on a layer of resist (ZEP-520A) to define the pattern. To combat the strong buckling of the silicon device layer by the compressive stress and upward turning moments of the oxide layer underneath, novel stress management techniques^{11,12} were incorporated to obtain structures with lithographically determined membrane-substrate gaps. After developing, a fluorine-based reactive-ion etch is employed to transfer the patterns to the top silicon layer. The device is then released by undercutting the patterned silicon layer with the vapor-phase hydrofluoric acid etch. Finally, an annealing step was performed at 500°C for 1 hour in a nitrogen environment to limit surface losses and maximize optical and mechanical quality factors. The height profiles of the released membranes from the substrate are characterized by a confocal microscope (Olympus LEXT OLS-4000).

The structure was designed to support an optical antibonding mode in the wavelength range of 1480-1680nm that results from the hybridization of waveguide modes in the membrane and substrate^{12,13}. The precise spectral location of the resonance is determined by the optomechanical coupling between the two modes, the strength of which is defined as $g_{OM} \equiv d\omega/ds$. The distribution of the x-component of the electric field in the top membrane is out-of-phase from that in the bottom membrane, as depicted in the simulation results of the whole structure in Fig. 1(b), which corresponds to the generation of a repulsive gradient force. Additionally, the field symmetries along the x-z and y-z planes indicate that we are operating with a “dark” mode^{14,15}, which theoretically does not couple to normally incident light because of mismatch in field symmetry. However, by breaking the periodicity of the full structure, we can couple to the dark mode and achieve high Q_{opt} . Such devices have been the subject of numerous theoretical and experimental investigations on subjects ranging from the lowering of the laser thresholds¹⁶ to increasing the sensitivity of photonic-crystal-based sensors¹⁷. Here, the dark mode is made accessible

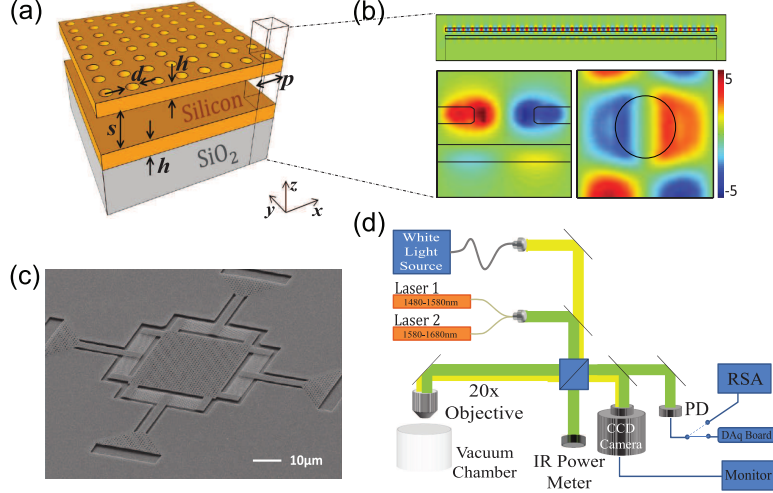


FIG. 1. (a) Schematic of membrane geometry consisting of a suspended silicon membrane above a silicon-on-insulator substrate. The top membrane is perforated by a 30×30 array of holes with diameter $d = 0.414 \mu\text{m}$ and period $p = 0.92 \mu\text{m}$. Both silicon layers have thickness $h = 185 \text{ nm}$. The width of the membrane is $27.6 \mu\text{m}$ on each side. (b) Top diagram shows the FDTD simulated E_x field profile for the antibonding mode at $\lambda_0 = 1584.85 \text{ nm}$ in the vertical cross-section of the full structure. Bottom left diagram shows the zoomed-in view of E_x field profile in the vertical cross-section of a unit cell. Bottom right diagram shows the E_x field profile in the horizontal cross-section of a unit cell, revealing the mode to be a dark mode. (c) An electron micrograph of a device. (d) Free-space coupling setup. A white-light source and output from a near-IR laser are combined and sent through a 50-50 beam splitter, sending half of the signal to an IR power meter and half through a 20x objective placed above a vacuum chamber. The reflected signal is sent back through the beam splitter and can be directed onto a CCD camera allowing us to carefully align the laser spot to the membrane and to a photodetector (PD) to collect optical spectra via the DAQ board and mechanical spectra via the real-time spectrum analyzer (RSA).

due to the finite size of the membrane and slight fabrication imperfection. The high Q_{opt} of the dark mode, together with the mode's large optomechanical coupling coefficient $g_{OM} = -2\pi \times 23 \text{ GHz/nm}$ (at $s_0 = 220.6 \text{ nm}$), boosts the strength of the optical force and hence the range of actuation.

As previously described¹⁰, the potential of a mechanical harmonic oscillator with

equilibrium position s_0 , when perturbed by the potential of an optical “spring”¹⁸ centered at s_l for a laser wavelength λ_l can create a multi-well potential with two stable mechanical equilibria. The transition between these mechanical equilibria is reflected by the occurrence of optical bistability, due to the dependence of the resonance frequency on s . Yet, the direct observation of the optomechanically-induced optical bistability can easily be obscured in actual systems by other competing mechanisms including thermo-optic effect due to two-photon absorption, free-carrier dispersion and the Kerr nonlinearity which otherwise have been actively pursued for realizing ultrafast, low-power optical switches and memory¹⁹. We designed our geometry to minimize these effects by exciting a guided resonance which is delocalized throughout the PhC membrane. We estimate the total mode volume to be $\approx 260(\lambda/n_g)^3$ from simulation. Due to its large modal volume, the thermal and electronic nonlinearities (which scale inversely with the modal volume) are dramatically reduced. This is in contrast with many of the optomechanical structures being studied, which have modal volumes $\approx (\lambda/n_g)^3$ and where thermal nonlinearities could be readily observed at even modest input powers. With the current membrane separation of the coupled PhC membrane, optomechanical detuning is larger than thermo-optic detuning that originates from linear absorption due to defects introduced during the fabrication processes, which is two orders of magnitude larger than the intrinsic material absorption of bulk silicon.

We solve for the the optical and mechanical equilibria in the presence of the thermo-optic effect within the coupled-mode theory framework²⁰. In particular, the stored optical energy in the system $|a|^2$ is given by

$$|a|^2 = \frac{\kappa_e}{(\kappa/2)^2 + \Delta^2} P_{in} \quad (1)$$

where κ is the full-width half-max linewidth of the optical resonance, κ_e is the ex-

ternal coupling rate such that κ_e/κ represents the fraction of incident power coupled into the cavity, and P_{in} is the power incident on the structure. Here the detuning Δ of the laser excitation frequency ω_l from the perturbed optical resonant frequency can be written as

$$\Delta = \omega_l - \omega_0 - (d\omega/dT)\Delta T - g_{OM}\Delta x. \quad (2)$$

The third term in Eq. 2 is the thermo-optic detuning, with $d\omega/dT = (d\omega/dn)(dn/dT)$, n is the refractive index of silicon, $d\omega/dn$ is obtained from simulations and approximately $-2\pi \times 10^{14}$ Hz and dn/dT is the thermo-optic coefficient of silicon equal to $2 \times 10^{-4} K^{-1}$.²¹ The absorbed optical power and hence the temperature change of the system is given by

$$\Delta T = \frac{\Gamma_{abs}|a|^2}{C_{th}\kappa_t} \quad (3)$$

where Γ_{abs} is the absorption coefficient of the system, C_{th} is the heat capacity, κ_t is the thermal diffusion rate. The fourth term in Eq. 2 is the optomechanical detuning. In particular, the displacement of the membrane due to the respective photo-thermo-mechanical force and the repulsive gradient force is given by

$$\Delta x = \frac{D\Delta T}{K} + \frac{|a|^2 g_{OM}}{\omega_l K} \quad (4)$$

where K is the spring constant of the mechanical resonator and D is the thermal-mechanical force coefficient in units of Newtons per Kelvin.²² The above equations can be solved self-consistently to yield Δ and hence the perturbed optical resonant frequency $\omega'_0 = \omega_0 + (d\omega/dT)\Delta T + g_{OM}\Delta x$ at a given ω_l and P_{in} .

The values of $\lambda'_0 = 2\pi c/\omega'_0$ at which solutions of Eq. 2 exist are plotted in Fig. 2(b), as a function of laser wavelength $\lambda_l = 2\pi c/\omega_l$ for incident powers of 0.275 (green

line), 0.775 (blue line), 1.275 (red line), 1.525 (purple line), 1.775 (orange line) and 2.275 mW (black line). The unperturbed optical resonance occurs at $\lambda_0 = 1581.55$ nm. The dashed portions of the curves correspond to unstable equilibria. At high powers, a clear bistable region exists in which there are two stable configurations of the membrane for fixed power and laser wavelength, due to both optomechanical and thermo-optic detunings whose magnitudes are comparable. The boundaries of the bistable region are denoted by λ_f and λ_b , representing the hysteretic transition wavelengths for a laser swept forward (left to right) and backward (right to left) across the resonance.

To investigate the hysteresis and bistability in our devices, we employ a free-space coupling setup in a low vacuum condition described in Fig. 1(d). A low power (25 μ W) wavelength sweep is shown in Fig. 2(a) (red curve), revealing a cavity resonance centered at $\lambda_0 = 1581.55$ nm. To account for interference fringes from parasitic reflections, we carefully fit both the optical resonance and the oscillating background (black line) to an expression which has the form

$$R = |r|^2 = \left| r_d(\lambda)e^{-i\phi} + \frac{\kappa_e}{-i\Delta'_0 + \kappa/2} \right|^2 \quad (5)$$

where $r_d(\lambda)$ is the background reflectivity, and ϕ is the relative phase between the underlying background reflection and the optical cavity. Fitting parameters correspond to an optical cavity with $\kappa_e = 0.3\kappa$ and $Q_{opt}^{tot} = \omega_0/\kappa = 3400$.

Using these parameters, we can model the reflectance of the system as a function of laser wavelength at multiple powers ($P = 0.275$ to 2.275 mW), shown in Fig. 3(a) and offset for clarity, and compare the results to our experimental observations, shown in Fig. 3(b). The experimental data were collected by sweeping the tunable laser output from short to long wavelength (red curve) and then back (blue curve)

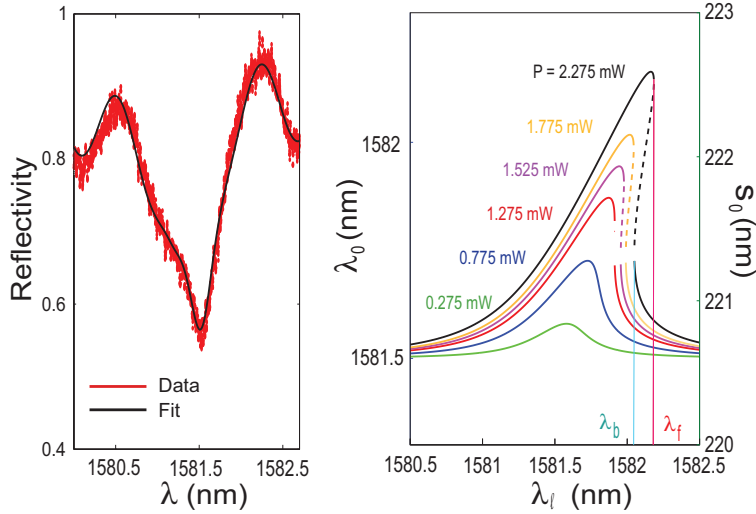


FIG. 2. (a) Reflection spectra of the device around the resonance centered at $\lambda_0 = 1581.55$ nm. (b) Calculated stable locations of the optical resonance as a function of laser wavelength, for six optical powers: 0.275 (green line), 0.775 (blue line), 1.275 (red line), 1.525 (purple line), 1.775 (orange line) and 2.275 mW (black line). At $P \geq 1.275$ mW, the system has three solutions (two stable – solid line, one unstable – dashed line) for a certain range of wavelengths. Due to the intracavity-power dependence of optical detunings from optomechanical and thermo-optic effects, the system is bistable in this wavelength range, and displays hysteresis when the laser is swept continuously from short to long wavelengths (forward sweep) or vice versa (backward sweep). Two hysteretic transition points occur at λ_f for the forward sweep and λ_b for the backward sweep.

at a fixed tuning speed of 1 nm/s. We find excellent agreement between experiment and theory, which display an overall redshift of the mode and increasing hysteresis at higher powers. In particular, we directly compare the locations of the forward and backward bistable jumps, λ_f and λ_b respectively, in Fig. 3(c). The locations of these transitions were extracted from the data shown in Fig. 3(b) by finding the minima of the reflectivities of forward and backward wavelength sweeps at each power. We see strong agreement between experiment (red/ blue circles) and theory (red/ blue line) on the locations of λ_f and λ_b .

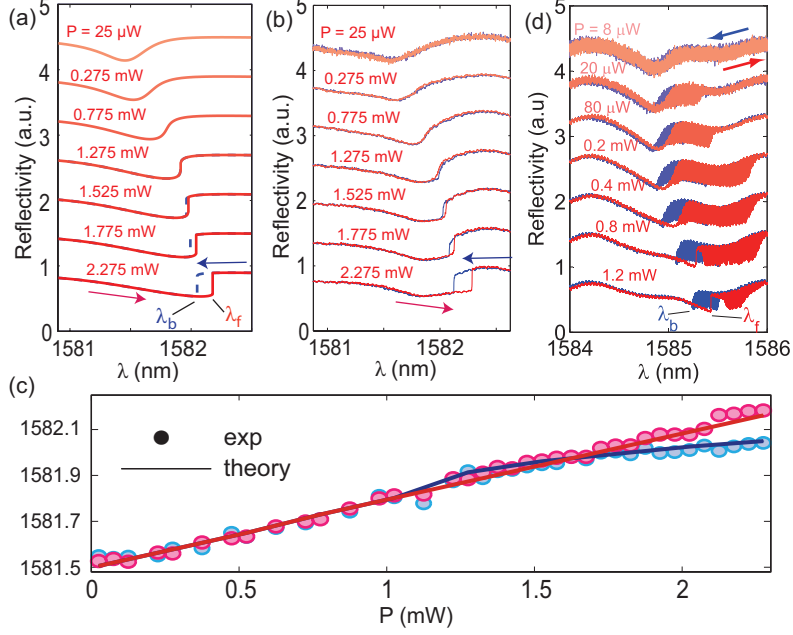


FIG. 3. Theoretical (a) and experimental (b) reflection spectra for forward (red lines) and backward (blue lines) swept lasers from $P = 0.275$ mW to 2.275 mW at *low vacuum*. Hysteresis is predicted to onset around 1.525 mW. (c) Locations of bistable transitions during forward and backward wavelength sweeps. The transition wavelength during the forward sweep λ_f (red circles) is linear, and matches well to theory (red line). The backward transition wavelength λ_b (blue circles) also show good agreement in the transition wavelength locations and the onset power for hysteresis. (d) Experimental reflection spectra for forward (red lines) and backward (blue lines) swept lasers from $P = 8 \mu\text{W}$ to 1.2 mW at *high vacuum*. Self-sustained oscillations occur on the red-detuned side of the resonances.

Alternately, we can investigate the range of actuation of the optical force by sweeping the *laser power* up and down at fixed wavelengths slightly red-detuned from the unperturbed cavity resonance. Theoretical predictions and experimental results are plotted in Fig. 4(a) and (b), respectively, showing the reflected power plotted against the incident laser power at nine red-detuned wavelengths: 1581.65 nm (black line), 1581.7 nm (grey line), 1581.75 nm (blue line), 1581.8 nm (cyan line), 1581.85 nm (green line), 1581.9 nm (magenta line), 1581.95 nm (violet line),

1582 nm (brown line), and 1582.05 nm (red line). The curves for the eight longer wavelengths are each vertically offset from the $\lambda_l = 1581.65$ nm curves for clarity. Again, we see good agreement between the calculated and experimental results: For small detunings ($\lambda_l = 1581.65$ to 1581.9 nm), the path traversed during an increase in input power from 0-2.25 mW (solid line) and a decrease in power (dashed line) coincide. At larger detunings, P_{out} experiences hysteresis. As the power is increased, the membrane enters the bistable region in the lower mechanical state and remains there until λ_b has redshifted such that $\lambda_b = \lambda_l$, at which point the membrane jumps to the lower curve, signifying an abrupt increase in the membrane separation. When decreasing the power, the membrane remains in the up-state until λ_f blue-shifts back to λ_l , forcing the membrane to jump to the upper curve which indicates an abrupt hop back to the pulled initial equilibrium position.

When we decompose the perturbation to the optical resonance into its constituent parts, we find optomechanically induced bistability to be the dominant effect. For example, at $P_{in} = 2.275$ mW, optomechanical effects correspond to a peak resonance shift $\Delta\lambda_{OM} = 0.44$ nm, while thermo-optic contributions lead to $\Delta\lambda_{PT} = 0.23$ nm and photo-thermal-mechanical contributions lead to $\Delta\lambda_{PTM} = -0.01$ nm. This corresponds to a membrane which is mechanically pushed upward 2.3 nm by the optical gradient force and 0.1 nm downward by the photo-thermal-mechanical force, resulting in a net maximum displacement of 2.2 nm. These results hold promise for large actuation range with repulsive optical forces by designing membranes which are less mechanically stiff and generate larger repulsive forces by increasing Q_{opt} . For instance, Q_{opt} is currently limited by fabrication imperfections and the finite size effect of the PhC and could be boosted by simply increasing the number of unit cells in the membrane¹⁶. To maintain the same compactness of the structure which is related to its dynamic range, the optical design could be modified with a smaller lattice constant and/ or graded hole modulation²³.

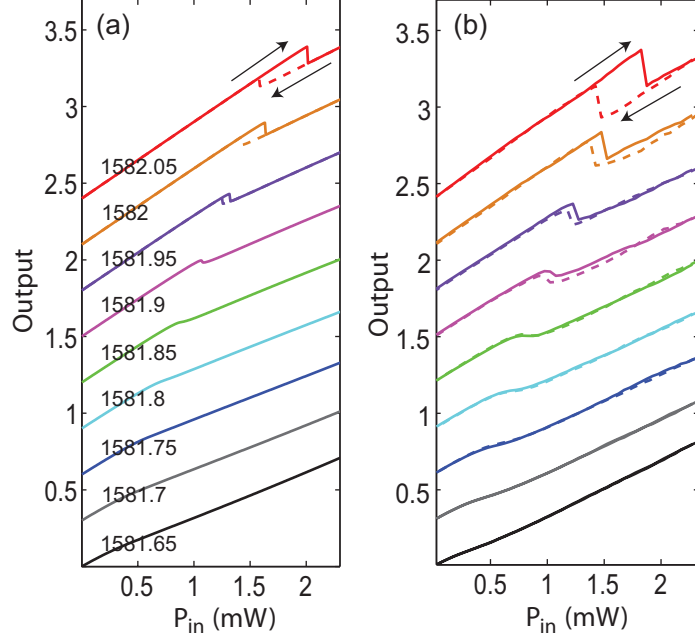


FIG. 4. Predicted (a) and experimental (b) P_{in} - P_{out} curves of the device. Curves (with equal offsets for illustration) are plotted for five red-detuned wavelengths: $\lambda = 1581.65$ nm (black line), 1581.7 nm (grey line), 1581.75 nm (blue line), 1581.8 nm (cyan line), 1581.85 nm (green line), 1581.9 nm (magenta line), 1581.95 nm (violet line), 1582 nm (brown line), and 1582.05 nm (red line). Solid lines represent the power output as a function of increasing laser power, while dashed lines represent power output as a function of decreasing input power. Modeling predicts hysteresis will occur at all wavelengths longer than 1581.95 nm.

Motivated by high-vacuum applications of on-chip manipulation of microscopic objects, we repeated the experiments above from $P = 8 \mu\text{W}$ to 1.2 mW at vacuum levels below 1 mTorr where self-sustained oscillations occur readily with a red-detuned excitation of moderate optical power. We examined the occurrence of optical bistability by sweeping the tunable laser output from short to long wavelengths and then back at the slowest tuning speed of 1nm/s. At 20 μW and higher, the PhC experiences self-sustained oscillations when the laser wavelength is red-detuned

$(\omega_l < \omega'_0)$ from the optical resonance due to positive feedback between Brownian motion of the membrane at its fundamental mechanical resonant frequency $\Omega_m = 180$ kHz and the thermomechanical force with a thermal diffusion rate $\kappa_t \approx 487$ kHz, taken from simulations and careful fitting to optical and mechanical spectra¹². This can be seen in Fig. 3(d) as the thick red and blue sections of the curves, corresponding to periodic oscillations of the reflectance at harmonics of Ω_m . Negative feedback between the membrane's motion and the photo-thermal-mechanical force occurs on the blue-detuned side of the resonance and works to damp the membrane oscillations²⁰, allowing us to adequately treat the system as static at these detunings. While the optical spring effect and dynamic back-action have been thoroughly investigated in our system¹², this paper focuses on evaluating the static effect of the repulsive optical and photo-thermo-mechanical forces. Qualitatively, we observe an overall redshift of the mode and increasing hysteresis at higher powers in Fig. 3(d). When we compare the bistable jump locations in both the forward and backward sweeps to the values calculated in the same coupled-mode model, the forward sweep data display good agreement while the backward sweep data show discrepancy in the transition wavelengths. We attribute this discrepancy to the fact that our static model does not include the dynamic back-action²⁰, which requires modeling over a wide range of time-scales spanning from the fundamental mechanical resonance frequency $\Omega_m = 180$ kHz to the optical frequency $\omega_0 = 189$ THz and is beyond the scope of this paper. Nevertheless, we can heuristically understand the effects of dynamic back-action as the cause of the discrepancy between our model and our experimental data due to detuning-dependent competition between mechanical amplification and cooling. The amplified mechanical oscillation corresponds to an oscillation of the optical resonance with an amplitude $\omega_{osc} = g_{OM}x_{osc}$ ($x_{osc} \approx 3.3$ nm; $\lambda_{osc} \approx 0.55$ nm) which is greater than κ . Thus, when ω_l is less than ω'_0 , the optical resonance oscillates such that it spends time on both sides of ω_l . In particular, when the resonance

experiences maximum red-shift, λ_l is greater than λ'_0 , leading to motion damping at this point in the oscillation. Thus, during a single oscillation cycle, the competing processes of cooling and amplification are occurring at different points in time. During the backward wavelength sweep, we argue that the system will transition from the amplified state into the cooled state (λ_b) before predicted by our static model, corresponding to the point at which cooling begins to dominate amplification over a single oscillatory cycle. Another caveat is that as the laser excitation is swept backward at the lowest sweeping speed such that the membrane transitions from an amplified state to a cooled state, the laser dwell time is shorter than the time needed for the membrane to equilibrate. Hence the backward bistable transition is obscured by the residual ringing in the optical spectra. As we relate this observation to our goal of optical actuation of mechanical resonators, it is sensible to traverse from the cooled state to an amplified state (which is the forward-sweep case here), whereas the reverse direction presents difficulties in evaluating the actuation range. Finally, we neglect the Duffing nonlinearity in our mechanical model as the oscillation amplitude is still well within the linear regime for our structures: The amplitude is much less than the membrane thickness ($185nm$) and the compressive stress in the silicon device layer is alleviated by thin accordion structures as shown in Fig. 1(c).

In conclusion, we demonstrated actuation of a micron-scale membrane with a repulsive optical force using an extended guided resonance in a coupled silicon PhC membrane. The net red-shift displayed in the optical resonance of our doubly-bonded SOI platform is a result of an optomechanically induced red-shift, a thermo-optic red-shift, and a photo-thermo-mechanically induced blue-shift. Furthermore, simulations indicate that absorption in our system is dominated by surface defects and adsorbents, resulting in a linear absorption coefficient two orders of magnitude larger than that expected from bulk silicon. By minimizing these effects through fabrication process and design modifications, we can further isolate and exploit the unique

optomechanical properties of this platform. Since multi-photon nonlinearities do not occur until the excitation power exceeds ≈ 1 W with the use of a delocalized optical mode, the extent of pulling of the PhC membrane can be many tens of nanometers. Our silicon-based device provides a simple, non-intrusive solution to extending the actuation range of MEMS devices.

The authors thank P. Deotare and I. Bulu for fruitful discussion. Devices were fabricated in the Center for Nanoscale Systems (CNS) at Harvard. This work was supported by the Defense Advanced Research Projects Agency (DARPA) under Contract No. N66001-09-1-2070-DOD.

REFERENCES

- ¹J. Chan, T. P. M. Alegre, A. H. Safavi-Naeini, J. T. Hill, A. Krause, S. Groblacher, M. Aspelmeyer, and O. Painter, *Nature* **478**, 89–92 (2011).
- ²A. G. Krause, M. Winger, T. D. Blasius, Q. Lin, and O. Painter, *Nature Photonics* **6**, 768–772 (2012).
- ³M. Hossein-Zadeh and K. J. Vahala, *Applied Physics Letters* **93** (2008).
- ⁴M. Davanco, J. Chan, A. H. Safavi-Naeini, O. Painter, and K. Srinivasan, *Optics Express* **20**, 24394–24410 (2012).
- ⁵Y. T. Yang, C. Callegari, X. L. Feng, K. L. Ekinci, and M. L. Roukes, *Nano Letters* **6**, 583–586 (2006).
- ⁶M. Eichenfield, R. Camacho, J. Chan, K. J. Vahala, and O. Painter, *Nature* **459**, 550–U79 (2009).
- ⁷G. S. Wiederhecker, L. Chen, A. Gondarenko, and M. Lipson, *Nature* **462**, 633–U103 (2009).
- ⁸M. L. Povinelli, M. Loncar, M. Ibanescu, E. J. Smythe, S. G. Johnson, F. Capasso, and J. D. Joannopoulos, *Optics Letters* **30**, 3042–3044 (2005).

- ⁹M. Li, W. H. P. Pernice, C. Xiong, T. Baehr-Jones, M. Hochberg, and H. X. Tang, *Nature* **456**, 480–U28 (2008).
- ¹⁰A. W. Rodriguez, D. Woolf, P. C. Hui, E. Iwase, A. P. McCauley, F. Capasso, M. Loncar, and S. G. Johnson, *Applied Physics Letters* **98** (2011).
- ¹¹E. Iwase, P. C. Hui, D. Woolf, A. W. Rodriguez, S. G. Johnson, F. Capasso, and M. Loncar, *Journal of Micromechanics and Microengineering* **22** (2012).
- ¹²D. N. Woolf, P. C. Hui, E. Iwase, M. Khans, A. W. Rodriguez, P. Deotare, I. Bulu, S. G. Johnson, F. Capasso, and M. Loncar, *Optics Express* **21**, 7258–7275.
- ¹³A. W. Rodriguez, A. P. McCauley, P. C. Hui, D. Woolf, E. Iwase, F. Capasso, M. Loncar, and S. G. Johnson, *Optics Express* **19**, 2225–2241 (2011).
- ¹⁴J. Lee, B. Zhen, S. L. Chua, W. J. Qiu, J. D. Joannopoulos, M. Soljacic, and O. Shapira, *Physical Review Letters* **109** (2012).
- ¹⁵O. Kilic, M. Dignonnet, G. Kino, and O. Solgaard, *Optics Express* **16**, 13090–13103 (2008).
- ¹⁶S. L. Chua, Y. D. Chong, A. D. Stone, M. Soljacic, and J. Bravo-Abad, *Optics Express* **19**, 1539–1562 (2011).
- ¹⁷M. El Beheiry, V. Liu, S. H. Fan, and O. Levi, *Optics Express* **18**, 22702–22714 (2010).
- ¹⁸B. S. Sheard, M. B. Gray, C. M. Mow-Lowry, D. E. McClelland, and S. E. Whitcomb, *Physical Review A* **69** (2004).
- ¹⁹P. B. Deotare, I. Bulu, I. W. Frank, Q. M. Quan, Y. N. Zhang, R. Ilic, and M. Loncar, *Nature Communications* **3** (2012).
- ²⁰T. J. Kippenberg and K. J. Vahala, *Science* **321**, 1172–1176 (2008).
- ²¹T. J. Johnson, M. Borselli, and O. Painter, *Optics Express* **14**, 817–831 (2006).
- ²²D. Blocher, A. T. Zehnder, R. H. Rand, and S. Mukerji, *Finite Elements in Analysis and Design* **49**, 52–57 (2012).
- ²³K. Srinivasan and O. Painter, *Optics Express* **10**, 670–684 (2002).